SAND2007-4739C

INTEGRATED LAYERED MANUFACTURING OF A NOVEL WIRELESS MOTION SENSOR SYSTEM WITH GPS

Misael Navarrete, Amit Lopes, Jacqueline Acuna, Raul Estrada, Eric MacDonald,
Jeremy Palmer*, and Ryan Wicker
The University of Texas at El Paso, W.M. Keck Center for 3D Innovation,
El Paso, Texas 79968

*Sandia National Laboratories
Albuquerque, New Mexico 87185-0958

Abstract

A programmable wireless motion sensor system with Global Positioning System (GPS) navigation capabilities was designed and manufactured for border security applications. The sensor was freeform manufactured using a previously developed layered manufacturing (LM) system that combines direct write (DW) conductive ink dispensing with stereolithography (SL). Electronic components were selected based on constraints imposed through the LM process and components included a low power rfPIC12F675K microcontroller with integrated radio frequency transmitter circuitry, Panasonic passive infrared motion sensor, and a Polstar GPS module. This circuit was selected to expand on the previously described capabilities of the hybrid SL/DW setup to fabricate three-dimensional (3D) circuits, and the circuit was designed for LM to include fewer external components, low voltage requirements (3V), simplicity to program the microcontroller, and represents a real wireless application. LM benefited the design and manufacturing of the sensor in comparison to traditional PCB manufacturing by (1) reducing the overall size of the sensor due to the 3D locations of components and circuitry, (2) allowing the overall shape of the sensor to change according to the environment in which it will be placed (so that it can take on the form of the local terrain, for example), and (3) providing a natural resistance to reverse engineering through 3D circuitry and component embedding.

Keywords: rapid prototyping; stereolithography; direct-write; hybrid integrated manufacturing; wireless sensor

Introduction

Illegal immigration within the United States (US) has become a very important political issue. Specifically, the southern border of the US with Mexico, which includes 1,951 miles of vast open desert with extreme high temperature conditions, presents a significant challenge for surveillance and control. Unattended motion sensors offer a potential solution by providing constant monitoring in remote and extreme environments and enable manpower to be used efficiently, reduce overall surveillance costs, and increase overall productivity of the security force while greatly assisting border security efforts. The functional requirements desired for an unattended sensor to be used for this type of application include:

- resistant to reverse engineering
- difficult to detect by violators
- high durability
- capable of operating in extreme (high) temperatures

- low maintenance requirements
- mobile
- self-locating

This paper proposes a wireless motion sensor with navigation capabilities via an onboard GPS receiver that communicates sensor activity and GPS data over an unregulated radio frequency (RF) transmission in an arbitrarily, 3D manufactured package designed to meet the functional requirements listed above. Recent advances in Rapid Prototyping of High Density Circuitry (RPHDC) research and, specifically, the development of a hybrid stereolithography and direct-write system (SL/DW) have enabled the fabrication of 3D structures with high-resolution electrically conductive media (Wicker *et al*., 2005). Stereolithography (SL) is one of the most widely used RP technologies to manufacture highly complex and accurate 3D prototypes due to its high build resolution. The use of different materials and the ability to build in arbitrary geometries can enable the design and manufacture of compact and visually appealing 3D circuits. Fabricating in several structured functional layers can reduce the overall circuit size and embedding the electronic components within the design can provide enhanced protection from harsh environments while increasing the overall strength and reliability of the final product (Lopes *et al*., 2006).

We have previously described a semi-automatic hybrid SL/DW manufacturing setup to enable research in these areas (Lopes *et al*., 2006). In this integrated manufacturing environment, SL is employed in conjunction with DW fluid dispensing technology to capitalize on each of the individual process capabilities for developing advanced electromechanical devices. Previous research determined that the DSM Somos® ProtoTherm™ 12120 resin (DSM Somos®, New Castle Delaware) provided the best resin alternative for the SL build due to its high heat deflection, relatively low viscosity, and its ability to build without sweeping (Lopes *et al*., 2006). The E1660 silver conductive ink (E1660-136, Ercon, Wareham, MA) was also shown to provide superior characteristics for the SL/DW application; it was initially selected due to its low curing temperature (138°C for 10 minutes), and its low resistivity (Lopes *et al*., 2006).

Using the SL/DW system, we successfully fabricated a fully functional LM555 temperature sensor circuit with embedded passive electrical components and DW interconnections between components as shown in Figure 1 (Lopes *et al*., 2006). The 555 timer circuit is based on the sequential charging and discharging of the external capacitor and can be used with a power supply in the range of 5-15 volts making it useful in many analog circuits. The simple temperature-sensitive circuit oscillated LEDs at a frequency proportional to the temperature sensed by the thermistor. Although this circuit served as a useful demonstration of the SL/DW process, there were several issues identified that required improvement before extending to more complex circuitry. For example, improved methods were required to accurately register the DW system with the embedded electronic components during changeover and a method was required to remove or cure uncured resin in component cavities prior to and after component insertion. In addition, although the E1660 ink was previously selected as the conductive media based on a simple resistivity

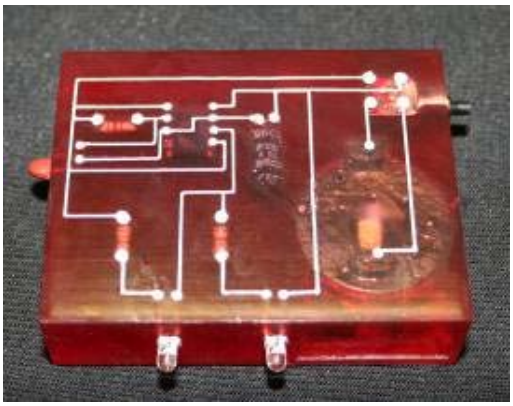

Figure 1. LM555 temperature circuit fabricated using the hybrid SL/DW setup.

experiment, further testing was required to measure impedances that arise in the conductive media when designing more complex 3D circuits. The following sections include descriptions of several improvements to the SL/DW process and the issues mentioned above with particular focus on applying this technology to a complex wireless motion sensor with navigation capabilities designed for a border security application.

SL/DW Building Constraints

In order to successfully design and build a circuit for LM, several considerations were made. These LM constraints, however, do not alter the performance of the overall circuit in either PCB or 3D, although they do help to simplify the design process and to successfully fabricate a 3D circuit. First, the number of components was minimized in order to reduce the requirements for component embedding. Second, the DW process imposed a minimum pitch requirement on the components. Using the smallest dispensing tip available (6-mil inner diameter), a DW ink trace of 8-mil width was achieved consistently. Therefore, trace width was limited to ~8-mil and the pin pitch spacing of the electronic components had to be greater than 8-mil. Finally, with SL, low powered and low frequency electronic components were preferred in order to minimize heat dissipation requirements as a result of component embedding (obviously, creative strategies can be employed for thermal management, but we elected to minimize heat load to reduce complexity of the design).

Motion Sensor Design

Hardware components for the motion sensor system architecture were selected based on the SL/DW manufacturing constraints mentioned previously and included additional selection criteria based on compatibility and cost. The rfPIC12F675K (Microchip Technology Inc., Chandler, Arizona) was selected as the microcontroller for the motion sensor due to its embedded RF circuitry and low power and cost. With the integration of RF circuitry in the microcontroller, components such as capacitors, inductors, filters and pre-amps were eliminated from the RF transmitter design. Although this integration proves useful during the 3D circuit design, other features were omitted from the microcontroller, which were useful in other areas such as Universal Synchronous Asynchronous Receiver Transmitter (USART). USART is needed for the rfPIC12F675K to communicate to a PC serial port and GPS module. The Polstar PGM-101 (Polstar Technologies, Hsinchu City, Taiwan) was selected as the GPS module. PGM-101 measures 27 X 27 X 9 millimeters and consumes 120 mW via a 3.3VDC. Passive infrared (PIR) sensors were chosen as the motion sensor system due to the wide motion sensing area and small size that allows them to be easily embedded in SL. The Panasonic MP1211 (Panasonic Electric Works Corporation of America, New Providence, New Jersey) has a motion sensing area of 110° at a maximum distance of 10 meters and requires 5V charge and 0.17μA current during operation. A block diagram of the motion sensor is illustrated in Figure 2.

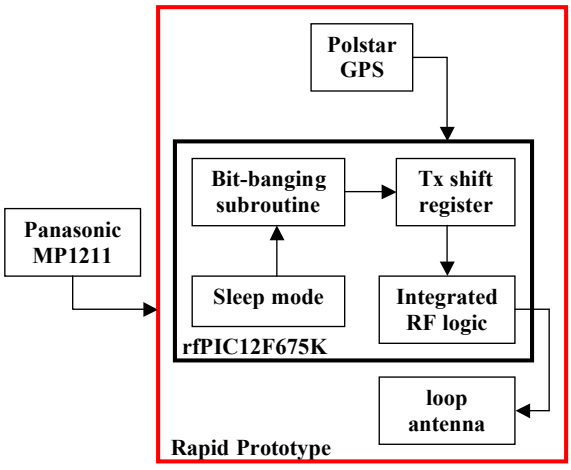

Figure 2. Motion sensor block diagram based on SL/DW building constraints.

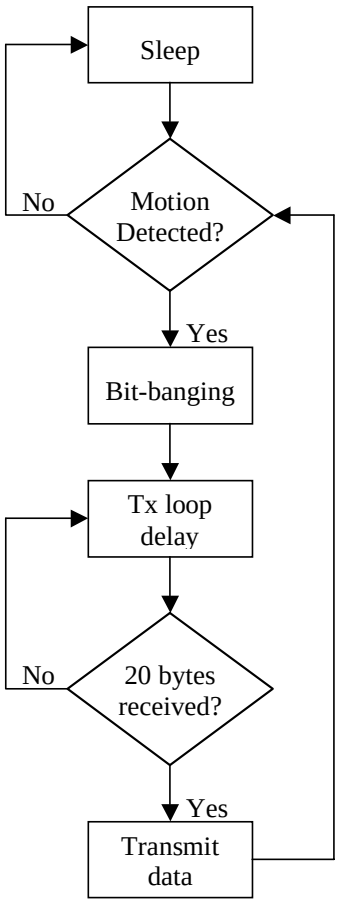

Figure 3. Motion sensor operation flowchart (software).

A considerable challenge faced during the development of the motion detection system was in the software programmed in the rfPIC12F675K. Due to the lack of a USART interface in the rfPIC12F675K, a 'bit-banging' subroutine was written for the rfPIC12 using Assembly Language. 'Bit-banging' is a technique created for facilitating serial communications to use software instead of dedicated hardware such as a USART or shift register. With a bit-banging program, the rfPIC12F675K will be able to communicate and receive serial data from the GPS receiver. A transmit code was written to initialize the transmission loop, Tx buffer and control the sleep mode of the rfPIC12F675K. Assembly Language was used to write the complete software for the rfPIC12F675K and burned via In-Circuit-Serial-Programming technique. Figure 3 shows a flow chart of the motion sensor software operation.

The Motion Sensor is initially in sleep mode to consume the least amount of current to prolong battery life. When motion is detected by a difference in infrared radiation, the PIR sensor sends a 'high signal' of V_{DD} to the rfPIC12F675K microcontroller interrupting it from sleep mode and calls the bit-banging subroutine. 20 bytes of NMEA format GPS coordinates are then transmitted at 315 MHz. NMEA is a standard protocol used by GPS receivers to transmit data.

PCB Demonstration

The software was debugged using MPLAB IDE v7.60 (Microchip Technology Inc., Chandler, Arizona) and voltages were measured at various points using a MeTex® multimeter

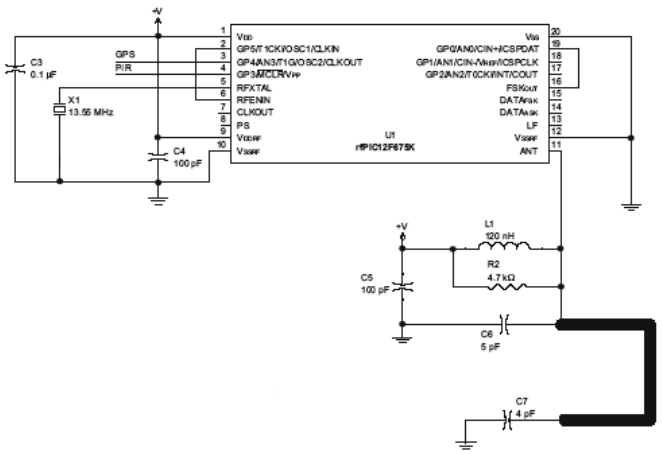

Figure 5. Motion sensor schematic with final component values.

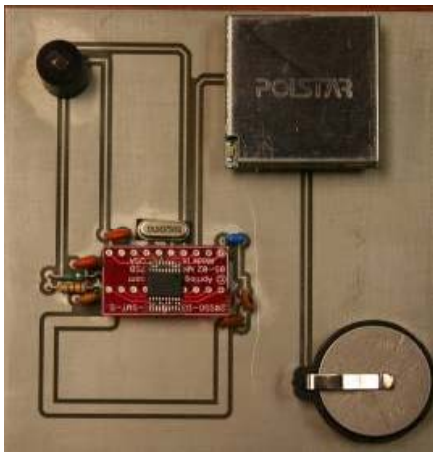

Figure 4. Fabricated PCB motion sensor.

(Model # M-3850D) to validate the motion sensor design. Once all software and components were operating as expected, a final schematic of the motion sensor was created as shown in Figure 4 and a PCB board was created as shown in Figure 5.

Two MeTex® multimeters (Model # M-3850D) and a Tektronix oscilloscope (Model # TDS 210) were used to check proper voltages and signal output in order to test the operation and transmission of the motion sensor. The output voltage of the PIR sensor was measured to check for 'high-low' (VDD to GND) voltage transition when motion was detected. The voltage at the RFENIN (Radio Frequency Enable Input) pin was measured to check if the pin went high (GRN to VDD) and enabled RF transmitter, and then whether the RFENIN pin went low after transmission, indicating that the rfPIC12F675K had changed to sleep mode disabling the transmitter. Oscilloscope probes were placed on ground and at the ANT (pin of the rfPIC12F675K to check whether the RF transmission was valid. The sensor was placed on the floor in a hallway with students walking by to activate the motion sensor, and the 20-byte GPS RF transmission was measured as shown in Figure 6 signifying that the motion sensor was operating as designed. When no motion was detected, the output signal had a signal of 0V indicating that no signal was being transmitted.

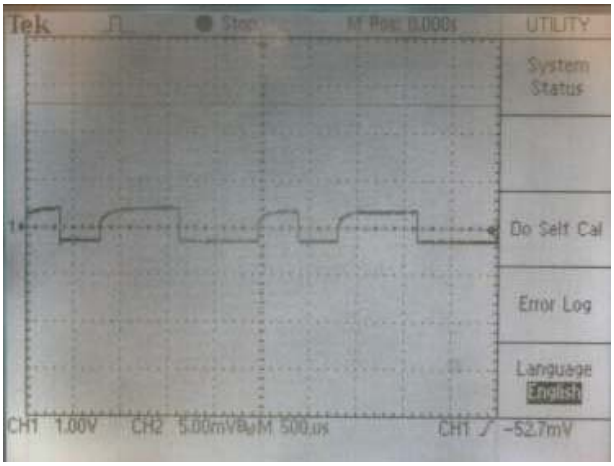

Figure 6. Measured antenna output of PCB motion sensor using two probe oscilloscope.

Designing for Layered Manufacturing

Through the work of Lopes *et al.* (2006), the comparison of average resistivity of various inks on different substrates determined that E1660 silver conductive ink had the lowest average resistivity after thermal curing. This conclusion was valid for low-voltage direct current (DC) circuits because frequency and high voltages were not considered. The motion sensor has several outputs with alternating voltage, thus indicating that there is a frequency factor that needs to be considered when evaluating potential conductive media and their parasitic losses. The capacitance reactance is known as X_C, inductive reactance is known as X_L and each is described by equations:

$$X_C = \frac{1}{2\pi * f * C} \qquad X_L = 2\pi * f * L$$

Capacitance impedes a change in voltage while inductance impedes a change in current. X_C is large at low frequencies and small at high frequencies, and at DC, X_C is infinite. The opposite is true for X_L. X_L is small at low frequencies and large at high frequencies, and at DC, X_L is zero. Therefore, in an AC circuit, one cannot ignore the frequency effects. Every wire, trace, component, or material experience these impedances, and whether these factors will significantly affect the performance of a circuit needs to be determined. To measure RLC values in various conductive media, SL parts with ink channels were designed using SolidWorks to obtain high RLC values. The CAD images of the three RLC tests are shown in Figure 7. The E1660 (E1660-136, Ercon, Wareham, MA), E1440 (E1400-136, Ercon, Wareham, MA), PTF-10A (PTF-10A, Advanced Conductive Materials Inc., Atascadero, Calif.), and CI-1001 (CI-1001, ECM LLC, Delaware, OH) were four inks chosen for the RLC test (see Lopes *et al.*, 2006, for a discussion of these inks). The channel width for this experiment was 0.010" (small enough for the pitch we were considering) and the channel depth was 0.004". The designed parts were sliced using the 3D Lightyear™ software and manufactured on a standard SLA 250/50 stereolithography machine. The RLC samples were cleaned and cured using Isopropyl alcohol. Using a direct application method, the ink was evenly applied into the groves by using a simple 'cotton cue-tip'. A paper sprayed with alcohol was used to remove the excess ink, while leaving the required ink into the channels. The samples were then placed in an oven at the manufacturer's recommended temperature for 10 minutes (cured samples shown in Figure 7).

(a) **(b)** **(c)**

Figure 7. Cured ink SL RLC test models; (a) Serpentine design increases resistance over length of ink line to allow for measurable data; (b) Coil design increases capacitance over length of ink line to allow for measurable data; (c) Loop design allows for the inductance of two adjacent ink lines to add while minimizing the attenuation of their magnetic field.

Since low RLC values were expected, a high resolution Agilent LRC Meter (Model # 4262B, Santa Clara, CA) was used to measure the RLC values of the SL test models. After initializing the LCR Meter with our initial test parameters (1 kHz, 1000mV, 0 m cable length), a 4-point

probe setup was used by connecting a Device Under Test (DUT) attachment. Under this test, any RLC value from the test probes will be automatically subtracted from any measurement as long as the test probes are within 1 meter length. The testing parameters R, C_P and L_P were selected and the test probes were placed at the opposite ends of the ink traces to measure the RLC values. Table I illustrates the measured RLC values that were used to calculate the reactance at 1 kHz frequency using the equations for X_C and X_L presented above. The calculated reactance of the various conductive inks is illustrated in Figures 8 and 9.

Table I. Measured RLC Values and Calculated Reactance.

PCB

Measured	1	2	3	4	Average	Calculated	1	2	3	4	Average
Capacitance (F)	-7.30E-06	-8.10E-06	-6.30E-06	-5.30E-06	-6.75E-06	XC (Ω)	21.813	19.659	25.276	30.044	24.198
Inductance (H)	4.60E-03	3.70E-03	4.90E-03	2.71E-03	3.98E-03	XL (Ω)	28.888	23.236	30.772	17.019	24.979
Resistance (Ω)	0.202	0.205	0.213	0.227	0.212						

E1660

Measured	1	2	3	4	Average	Calculated	1	2	3	4	Average
Capacitance (F)	-4.10E-06	-4.40E-06	-3.10E-06	-1.90E-06	-3.38E-06	XC (Ω)	38.838	36.190	51.366	83.808	52.551
Inductance (H)	7.90E-03	6.10E-03	8.00E-03	9.10E-03	7.78E-03	XL (Ω)	49.612	38.308	50.240	57.148	48.827
Resistance (Ω)	0.315	0.298	0.304	0.298	0.304						

E1400

Measured	1	2	3	4	Average	Calculated	1	2	3	4	Average
Capacitance (F)	-8.57E-07	-2.00E-06	-8.57E-07	-1.30E-06	-1.25E-06	XC (Ω)	185.741	79.618	185.893	122.489	143.435
Inductance (H)	1.94E-02	2.48E-02	3.13E-02	1.11E-02	2.17E-02	XL (Ω)	121.832	155.744	196.564	69.708	135.962
Resistance (Ω)	0.574	0.785	0.646	0.434	0.609						

PTF-10A

Measured	1	2	3	4	Average	Calculated	1	2	3	4	Average
Capacitance (F)	-5.32E-07	-6.46E-07	-5.93E-07	-4.73E-07	-5.61E-07	XC (Ω)	299.146	246.686	268.390	336.508	287.683
Inductance (H)	2.82E-02	3.96E-02	4.64E-02	7.01E-02	4.61E-02	XL (Ω)	177.347	248.688	291.392	440.228	289.414
Resistance (Ω)	0.693	0.889	0.824	0.984	0.848						

CI-1001

Measured	1	2	3	4	Average	Calculated	1	2	3	4	Average
Capacitance (F)	-2.36E-07	-2.03E-07	-2.23E-07	-2.19E-07	-2.20E-07	XC (Ω)	673.871	784.412	714.061	727.104	724.862
Inductance (H)	1.47E-01	1.68E-01	1.41E-01	1.82E-01	1.59E-01	XL (Ω)	920.648	1056.924	887.364	1141.076	1001.503
Resistance (Ω)	1.400	1.590	1.560	1.500	1.513						

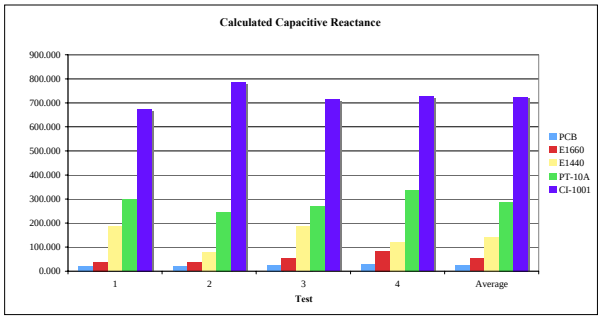

Figure 8. Capacitive Reactance.

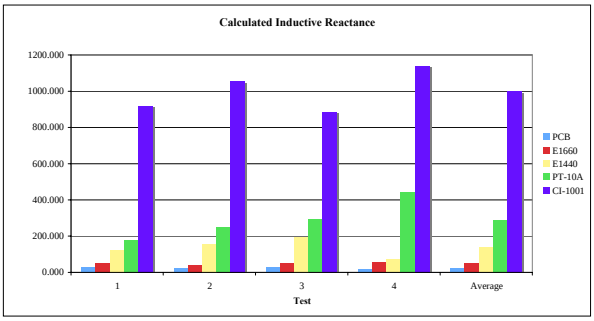

Figure 9. Inductive Reactance.

In all the parasitic measurements, the E1660 silver conductive ink was within 10% of the industry standard PCB making it the best choice for electrical interconnects in the SL/DW setup. The reactance measurements for the remaining inks were too high, potentially having serious attenuation effects on the circuit, and therefore were no longer considered as candidates for electrical interconnects.

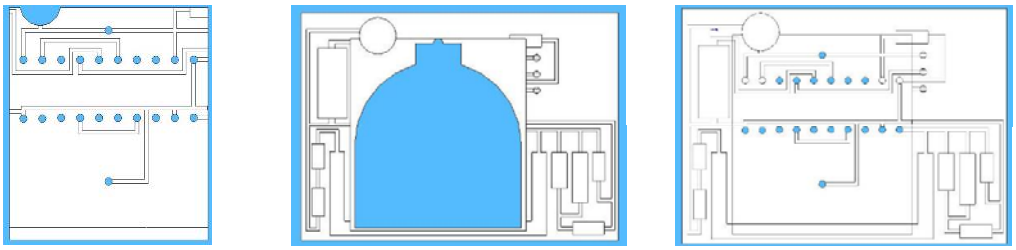

(a) (b) (c)

Figure 10. SolidWorks motion sensor assembly design; (a) part I of the motion sensor design includes most ink channels and houses the rfPIC12F675K cavity; (b) part II of the motion sensor includes most electrical components and houses the battery cell cavity; (c) complete assembly of the motion sensor.

Assembly for Layered Manufacturing

To fabricate the motion sensor in a 3D design, the PCB schematic was considered as a 3D model divided into several integrated sections. Each component was given a location and orientation based on the proximity to the rfPIC12F675K. The final 3D motion sensor was designed in an assembly of parts using SolidWorks modeling software. By creating multiple parts that snap together, components were packaged closer together, which resulted in smaller complex designs. The SolidWorks assembly model of the motion sensor is shown in Figure 10. DSM Somos® ProtoTherm™ resin, E1660 conductive ink and the hybrid SL/DW system was used to fabricate the 3D motion sensor. The SL/DW process was initiated by building the SL base with sockets, ink channels and vias at set parameters for inserting the electronic components. Once the SL parts were built, they were removed from the platform and the sockets, ink channels and vias were cleaned prior to inserting the electronic components. The components were manually inserted into their respective sockets and the connector pins of the components were placed into their pre-fit vias in the ink channel. Once all components and connector pins were inserted, the SL motion sensor parts were assembled together as shown in Figure 11.

After completing the ink deposition, the motion sensor was cured using a heat convection oven set at 138 ˚C for 10 minutes. The total time to manufacture the 3D motion sensor with embedded components and DW interconnections was approximately one and a half hours. The functional hybrid SL/DW part was further compared to the PCB motion sensor for functionality.

Figure 11. Fabricated SL motion sensor based on an assembly design.

Demonstration

Since all components were embedded, it was difficult to test voltages and output signals of the motion sensor using multimeters and oscilloscopes without damaging the circuit. Therefore, to test the 3D motion sensor, a Graphical User Interface (GUI) and a receiver circuit were developed. The receiver setup collected any information transmitted from the sensor once motion was detected, converted the information to Recommended Standard 232 (RS232), and displayed the GPS coordinates in NMEA format in the GUI application. To simulate this, a laptop with the GUI and receiver setup were placed 10 meters from the motion sensor outside in an open field. As a person walked past the motion sensor, movement was detected and the GPS data were successfully displayed on the GUI application as shown in Figure 12.

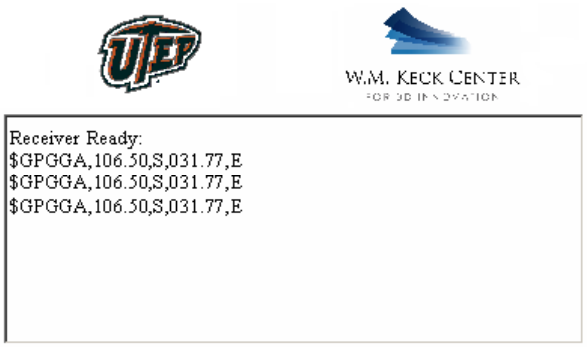

Figure 12. 20 bytes of NMEA GPS data received after motion sensor was triggered; data is displayed via a GUI application.

Conclusion

A wireless motion sensor with GPS navigation was designed based on functional requirements and SL/DW building constraints. A PCB version of the motion sensor was fabricated and tested in order to test the operation of the motion sensor. A 3D model was proposed to incorporate the functional requirements of the motion sensor. In order to achieve accurate transmission of information in complex circuitry (with fluctuating voltages and currents), a suitable conductive media for DW with parasitic values comparable to copper traces was desired. An RLC test was performed using SL parts designed to obtain high parasitic values. Four DW inks were dispensed using a direct application method and cured at the recommended curing conditions. An LCR Meter was used to measure resistance, capacitance, and inductance at 1 kHz frequency and reactance was calculated using standard capacitive and inductive equations. E1660 from Ercon Inc., Wareham, MA was found to have the most comparable RLC values to copper traces and was chosen as the DW ink. To fabricate the sensor, an assembly of parts was designed using SolidWorks in order to achieve the most compact design to fabricate a 3D motion sensor suitable for layered manufacturing. A hybrid SL/DW machine setup was used for manufacturing embedded electronic components in a semi-automated environment with DW interconnects. A GUI and a receiver circuit were designed to test the performance of the 3D motion sensor and both the PCB and 3D circuits showed similar performance.

Acknowledgments

The facilities within the W.M. Keck Center for 3D Innovation (Keck Center) used here contain equipment purchased through Grant Number 11804 from the W.M. Keck Foundation, a faculty STARS Award from the University of Texas System, and two equipment grants from Sandia National Laboratories. This material is based in part upon work supported through the Mr. and Mrs. MacIntosh Murchison Chair I in Engineering and through research contract 504004 from Sandia National Laboratories in the Laboratory Directed Research and Development

(LDRD) program. Sandia National Laboratories is a multi-program laboratory operated by Sandia Corporation, a Lockheed Martin Company, for the United States Department of Energy's National Nuclear Security Administration under contract DE-AC04-94AL85000.

References

1. A.J. Lopes, M. Navarrete, F. Medina, J.A. Palmer, E. MacDonald, R.B. Wicker, "Expanding Rapid Prototyping for Electronic Systems Integration of Arbitrary Form", *Proceedings of the 2006 Solid Freeform Fabrication*, Austin, Texas, 2006.
2. D. Begaye, "Optical Transmission on Digital Signals through Rapid Prototyping Fibers", 2003 National Conference on Undergraduate research, Salt Lake City, Utah.
3. DSM Somos, June 2002, *ProtoTherm 12120 –Product Data Sheet*, New Castle: Delaware, www.dsmsomos.com, 03/27/2005.
4. ECM LLC, 2004, *CI-1002 – Product Data Sheet*, Delaware, Ohio, www.conductives.com, 06/15/2005.
5. F. Medina, A.J. Lopes, A.V. Inamdar, R. Hennessey, J.A. Palmer, B.D. Chavez, and R.B. Wicker, "Integrating Multiple Rapid Manufacturing Technologies for Developing Advanced Customized Functional Devices," *Rapid Prototyping & Manufacturing 2005 Conference Proceedings*, Rapid Prototyping Association of the Society of Manufacturing Engineers, May 10-12, 2005, Hyatt Regency Dearborn, Michigan.
6. F. Medina, A.J. Lopes, A.V. Inamdar, R. Hennessey, J.A. Palmer, B.D. Chavez, D. Davis, P. Gallegos, and R.B. Wicker, "Hybrid Manufacturing: Integrating Direct-Write and Stereolithography", *Proceedings of the 2005 Solid Freeform Fabrication*, Austin, Texas, 2005.
7. R. Mosses; S. Brackenridge, "A Novel Process for the Manufacturing of Advanced Interconnects", *Circuit World*, Volume 29, Number 3, 2003, pages 18-21.
8. T. F. L. Ocampo, "Incorporation of Electrical Components into Rapid Prototyped Products", 2003 National Conference on Undergraduate Research, Salt Lake City, Utah.
9. J.A. Palmer, P. Yang, D.W. Davis, B.D. Chavez, P.L. Gallegos, R.B. Wicker, and F.R. Medina, "Rapid Prototyping of High Density Circuitry," *Rapid Prototyping & Manufacturing 2004 Conference Proceedings*, Rapid Prototyping Association of the Society of Manufacturing Engineers, May 10-13, 2004, Hyatt Regency Dearborn, Michigan. Also, *SME Technical Paper TP04PUB221* (Dearborn, Michigan: Society of Manufacturing Engineers, 2004).
10. J.A. Palmer, J.L. Summers, D.W. Davis, P.L. Gallegos, B.D. Chavez, P. Yang, F. Medina, and R.B. Wicker, "Realizing 3-D Interconnected Direct Write Electronics within Smart Stereolithography Structures," *International Mechanical Engineering Congress and Exposition 2005 Proceedings*, November 14-18, 2005, Orlando, Florida.